JOURNAL OF AGRICULTURAL AND FOOD CHEMISTRY

Article

Mitochondrial Signs and Subcellular Imaging Imply the Antifungal Mechanism of Carabrone against *Gaeumannomyces graminis* var. *tritici*

Lanying Wang, Yunfei Zhang, Delong Wang, Mei Wang, Yong Wang, and Juntao Feng

J. Agric. Food Chem., **Just Accepted Manuscript** • DOI: 10.1021/acs.jafc.7b03913 • Publication Date (Web): 12 Dec 2017

Mitochondrial Signs and Subcellular Imaging Imply the Antifungal Mechanism of Carabrone against *Gaeumannomyces graminis* var. *tritici*

Lanying Wang,[†,‡] Yunfei Zhang,[†] Delong Wang,[†] Mei Wang,[†] Yong Wang,[†] and Juntao Feng*[,†,#]

[†]Research and Development Center of Biorational Pesticide, Northwest A&F University, Yangling 712100, Shaanxi, China

[‡]Institute of Tropical Agriculture and Forestry, Hainan University, Haikou 570228, Hainan, China

[#]Engineering and Research Center of Biological Pesticide of Shaanxi Province, Yangling 712100, Shaanxi, China

ABSTRACT: Carabrone, a botanical bicyclic sesquiterpenic lactone, has broad-spectrum antifungal activities, and is particularly efficient against the devastating phytopathogen *Gaeumannomyces graminis* var. *tritici* (Ggt). The antifungal mechanism of carabrone against Ggt, however, remains unclear. The main objective of this study was to investigate the subcellular localization of carabrone in Ggt to make a better understanding of the mechanism of action. When Ggt was exposed to carabrone (EC_{50} value, 28.45 μg/mL) for 7 days, the decline of mitochondrial concentration, together with some obvious alternations in the mitochondrial structure including hazy outline, medullary transition, excess accumulation of unclear settlings, and vacuolar degeneration were observed, indicating that carbrone may act on the mitochondria directly. A fluorescent conjugate (TTY) was thus designed and synthesized as a surrogate of carabrone, which possessed comparable antifungal activity against Ggt (EC_{50}, 33.68 μg/mL). Meanwhile, polyclonal antibody specific to carabrone with a high titer (256,000) was also prepared by immunizing mice. Subsequently, two imaging techniques, fluorescent conjugate (FC) and immunofluorescence (IF), were applied to determine the subcellular localization of carabrone. Both FC and IF fluorescent signals demonstrated its mitochondrial localization with a Pearson's coefficient of 0.83 for FC, and 0.86 for IF. These results imply that carabrone exerts its antifungal activity against Ggt by interference with mitochondrial functions.

KEYWORDS: carabrone, fluorescent conjugate, polyclonal antibody, immunofluorescence, subcellular localization, mitochondria, *Gaeumannomyces graminis var. tritic*

34 **INTRODUCTION**

35 Take-all, a worldwide soil-borne disease of wheat caused by *Gaeumannomyces graminis*
36 var. *tritici* (Ggt), severely affects global wheat production, which can bring about serious
37 yield and economic losses in epidemic years.[1, 2] The traditional control methods are often
38 limited in practical application by lack of resistant cultivar,[1, 3] inefficiency of crop rotation
39 and tillage management measures,[4] poor robustness of take-all decline,[4] as well as
40 environmental concerns and fungicide resistance issues related to chemical fungicides.[5]
41 Biocontrol agents[6] and botanical fungicides[7] have been recognized as safer and more
42 effective alternatives than conventional strategies. To date, microorganisms such as
43 *Pseudomonads*[8, 9] and *Bacillus* species[10, 11] have been developed as biocontrol agents
44 against take-all. However, natural chemical compounds effective against Ggt is rarely
45 reported.[12]

46 Carabrone (Figure 1), a bicyclic sesquiterpenic lactone isolated from the fruits of
47 *Carpesium abrotanoides*, is widely distributed in feverfew and other plant species,[13] and
48 exhibits diverse bioactive properties including antibacterial,[14, 15] and antitumor activities.[16]
49 It has been reported that carabrone possessed a broad-spectrum antifungal activity, and that
50 it was more effective against Ggt than other phytopathogens tested, with a EC_{50} value of
51 28.45 μg/mL.[17] Although carabrone has a great potential to be developed as an effective
52 antifungal agent for take-all control, the antifungal mechanism of carabrone against Ggt
53 still remains unclear.

54 A vast array of sesquiterpene lactones depend on a α-methylene-γ-butyrolactone
55 structural motif to exert their biological activities, which may play a pivotal role in

56 mediating the interaction with unidentified target molecule(s).[18, 19] In addition, a range of
57 natural lactones, such as britannin,[20] arucanolide,[21] parthenolide,[22] costunolide,[23] and
58 isocostunolide[24] have been proved to involve in intracellular mitochondria-related
59 pathways to induce apoptosis of cancer cells (Figure 1). Given the identical
60 α-methylene-γ-butyrolactone substructure, we speculated that carabrone might also exert
61 its antifungal activity against Ggt via targeting the mitochondria (Figure 1). Our previous
62 studies also indicated that carabrone inhibited not only the intracellular oxidation process,
63 but also the activity of respiratory chain complexes I-V in Ggt.[25, 26] Nonetheless, direct
64 evidences supporting this hypothesis are still lacking.

65 Imaging techniques such as immunofluorescence (IF)[27, 28] and synthesis of fluorescent
66 conjugate (FC)[29, 30] are widely used to investigate the subcellular distribution of bioactive
67 molecules with high spatial and temporal resolution, and the action mechanisms of the
68 corresponding molecules could be inferred based on these techniques.[31-33] In order to verify
69 our hypothesis (Figure 1) proposed above, we first examined the changes in mitochondrial
70 ultrastructure and concentration of Ggt hyphae exposed to carabrone. Subsequently, we
71 designed and synthesized a fluorescent-labeled carabrone analog TTY, and generated the
72 polycolonal antibody against carabrone. After investigating their properties suitable for cell
73 imaging, they were used to image the subcellular localization of carabrone in Ggt by IF
74 and FC techniques.

75 **MATERIALS AND METHODS**

76 **General Information.** The carabrone compound characterized in this study was isolated
77 from *Carpesium macrocephalu* and purified (> 98% in purity) in our laboratory. NMR

78 spectra were recorded on a Bruker AVANCE III 500 spectrometer (Germany) with
79 tetramethylsilane as internal standard. The mass spectra (MS) of new compounds were
80 obtained by a LCQ Fleet mass spectrometer (USA). *N*-Methyl anthranilic acid (NAA,
81 98%), carboxymethoxylamine hemihydrochloride (99%), *N*-Hydroxysuccinimide (NHS,
82 98%), ethylenediamine (99%), 4-dimethylaminopyridine (DMAP, 98%), *N*,
83 *N*-Dicyclohexylcarbodiimide (DCC, 97%),
84 1-(3-Dimethylaminopropyl)-3-ethylcarbodiimide hydrochloride (EDC, 98%), isobutyl
85 chloroformate (98%), tributylamine (97%), and tetramethylbenzidine (TMB, 98%) were
86 purchased from Aladdin Co. Ltd. (Shanghai, China). Bovine albumin (BSA), ovalbumin
87 (OVA), incomplete Freund's adjuvant (IFA), complete Freund's adjuvant (CFA), tween-20,
88 tritonX-100, parafomaldehyde, HRP-labeled Goat Anti-Mouse IgG(H+L), anti-Mouse IgG
89 (whole molecule)-FITC, cellulase, driselase, and lyticase were purchased from
90 Sigma-Aldrich (USA). MitoTrackerR Green FM (M7514), and MitoTrackerR Red
91 CMXRos (M7512) were purchased from Invitrogen (USA). RedDot™1 (200X) was
92 obtained from Biotium (USA). All organic solvents were commercial AR solvents and
93 were purified when necessary. Silica gels for TLC and column chromatography were
94 obtained from Qingdao Haiyang Chemical Co. Ltd (Qingdao, China).

95 **Synthesis of Fluorescent-labeled Carabrone (TTY).**
96 *2-(((4-(5a-methyl-3-methylene-2-oxooctahydro-2H-cyclopropa[f]benzofuran-5-yl)butan-2-*
97 *ylidene) amino)oxy)acetic acid (HH1).* HH1 was prepared according to the reported
98 method[34] with some modifications. For details, carboxymethoxylamine hydrochloride
99 (196.82 mg, 2.4 mmoL, 1.2 equiv) and sodium acetate (1.2 equiv) were successively added

100 to a solution of carabrone (1.0 equiv) in 20 mL 95% ethanol. The reaction mixture was
101 stirred at room temperature under nitrogen for 12 h. After that, the resultant mixture was
102 filtered, evaporated, and purified by column chromatography on silica gel (80-100 mesh)
103 using petroleum ether/ethyl acetate/acetic acid (2/1/0.05, v/v/v) as the eluate to yield HH1.
104 Colorless oil: yield 90.3%. ^{1}H NMR (500 MHz, CD_3OD) δ 6.17 (d, *J* = 2.0 Hz, 1H), 5.68
105 (d, *J* = 2.0 Hz, 1H), 4.53 (d, *J* = 11.5 Hz, 2H), 3.30 – 3.19 (m, 1H), 2.50 (t, *J* = 7.6 Hz, 1H),
106 2.45 – 2.35 (m, 1H), 2.24–2.32 (m, 3H), 1.90 (d, *J* = 25.2 Hz, 3H), 1.66 – 1.56 (m, 1H),
107 1.51 (dq, *J* = 14.8, 7.5 Hz, 1H), 1.12 (dd, *J* = 10.8, 5.6 Hz, 4H), 0.99 (m, 2H), 0.62 – 0.52
108 (m, 1H), 0.51 – 0.39 (m, 1H); ^{13}C NMR (125 MHz, MeOD) δ 171.31, 159.94, 159.44,
109 139.72, 121.69, 76.33, 69.43, 37.61, 36.82, 35.03, 33.95, 30.36, 25.60, 22.97, 16.55, 13.15;
110 ESI-MS, *m/z* 322.2 $[M+H]^+$.

111 *N-(2-(2-(((4-(5a-methyl-3-methylene-2-oxooctahydro-2H-cyclopropa[f]*
112 *benzofuran-5-yl)butan-2-ylidene)amino)oxy)acetamido)ethyl)-2-(methylamino) benzamide*
113 *(TTY).* The synthetic procedures of TTY were modified according to the literature.[35, 36]
114 *N*-methyl anthranilic acid (TY, 302.3 mg, 2 mmoL, 1 equiv) was dissolved in 20 mL dry
115 CH_2Cl_2, to which NSH (1.5 equiv) and catalytic amount of DMAP (0.1 equiv) were added.
116 After cooling to 0°C, a solution of DCC (1.5 equiv) in 10 mL anhydrous CH_2Cl_2 was
117 added dropwise into the mixture. The reaction mixture was stirred at 0°C for 45 min and
118 then stirred at room temperature for another 16 h. The mixture was filtered and the filtrate
119 was washed with 0.05 N HCl (10 mL × 2) and brine. The organic layer was dried over
120 anhydrous Na_2SO_4, filtered and evaporated by a rotary evaporator to yield **1**. Compound **1**
121 obtained was dissolved in 20 mL dry CH_2Cl_2 and the resulting solution was added

122 dropwise to 10 mL anhydrous CH_2Cl_2 with 41.33 mmoL of ethylenediamine (2.75 mL)
123 over 30 min. The mixture was stirred at room temperature under nitrogen for 24 h, and
124 then filtered and washed with brine (100 mL × 3). The organic layer was dried over
125 anhydrous Na_2SO_4, filtered, concentrated, and purified by chromatography on silica gel
126 (80-100 mesh) using dichloromethane/ethanol/ammonium hydroxide (30/1/0.05, v/v/v) as
127 the eluate to yield HH2. HH1 (250 mg, 0.78 mmoL, 1 equiv), EDC (1.2 equiv) and DMAP
128 (0.1 equiv) were dissolved in anhydrous CH_2Cl_2 (30 mL) and stirred at 0°C for 30 min.
129 Then, a solution of HH2 (1.5 equiv) in anhydrous CH_2Cl_2 (10 mL) was added dropwise to
130 the mixture within 30 min. The reaction mixture was stirred at room temperature for
131 another 24 h and then filtered, concentrated, and purified by chromatography on silica gel
132 (80-100 mesh). Elution with petroleum ether/ethyl acetate/ammonium hydroxide (1/5/0.05,
133 v/v/v) gave the pure compound TTY. Slightly yellow oil: yield 61.7%. The fluorescent
134 properties of compound TTY *in vitro* were monitored using a F-4500 fluorescence
135 spectrophotometer (Hitachi, Japan) with the scanning mode, 250-400 nm for excitation
136 spectrum, and 415-800 nm for emission spectrum. ^{1}H NMR (500 MHz, $CDCl_3$) δ 7.56 (s,
137 1H), 7.41 (dd, J = 7.8, 1.1 Hz, 1H), 7.33 (t, J = 7.8 Hz, 1H), 7.29(s, 1H), 7.28(s, 1H), 6.67
138 (d, J = 8.4 Hz, 1H), 6.61 (t, J = 7.5 Hz, 1H), 6.25 (d, J = 2.3 Hz, 1H), 5.57 (d, J = 2.3 Hz,
139 1H), 4.85-4.69 (m, 1H), 4.52 (s, 2H), 3.56 (s, 3H), 3.16 (dt, J = 11.6, 9.0 Hz, 1H), 2.87 (s,
140 3H), 2.32 (ddd, J = 20.1, 13.9, 6.4 Hz, 2H), 2.25-2.18 (m, 2H), 1.93 (s, 3H), 1.54 (dt, J =
141 14.3, 7.1Hz, 1H), 1.48-1.37 (m, 1H), 1.28 (t, J = 7.1 Hz, 1H), 1.07 (s, 3H), 1.05-0.88 (m,
142 2H), 0.41 (dt, J = 11.2, 5.7 Hz, 1H), 0.38-0.32 (m, 1H); ^{13}C NMR (125 MHz, $CDCl_3$) δ
143 171.69, 170.72, 170.63, 160.08, 150.60, 139.09, 132.98, 127.59, 122.72, 114.69, 114.46,

144 111.04, 75.72, 72.45, 40.26, 39.59, 37.52, 37.10, 35.64, 33.89, 30.61, 29.68, 25.87, 22.83,
145 18.36, 17.09, 14.56; ESI-MS, *m/z* 497.3 $[M+H]^+$.

146 **Preparation of Immunogen and Coating Antigen.** Immunogen (T-BSA) was
147 synthesized according to the method described by Wang et al. with slight modification.[37]
148 Hapten (HH1, 15.6 mg, 0.048 mmoL) was dissolved in 1.0 mL of dry DMF containing
149 0.28 mmoL of NSH. The mixture was stirred for 15 min at room temperature and 0.20
150 mmoL of DCC was added. After stirring in the dark for 5 h, the reaction mixture was
151 centrifuged (10,000 rpm, 10 min, 4°C) to remove the precipitate. The resulting supernatant
152 was added slowly to 5 mL carbonate buffer (50 mM, pH 9.6) with 50 mg BSA under
153 magnetic stirring at 0°C within 30 min. After dropping, the reaction continued for 6 h
154 under the same conditions and purified by dialyzing extensively with phosphate buffer
155 saline (PBS, 10 mM, pH 7.4) for 3 days at 4°C. The purified T-BSA solution was
156 lyophilized and kept at -20°C for use.

157 The preparation of coating antigen (T-OVA) was according to Gendloff et al.'s method[38]
158 with some revisions. Briefly, 15.6 mg of HH1 was dissolved in 1 mL dry DMF and cooled
159 to 0°C. To this, 77 μL tri-*n*-butylamine and 22 μL isobutyl chloroformate were added and
160 the mixture was stirred at room temperature for 5 h. After cooling to 0°C, the mixture was
161 added dropwise to a stirring mixture solution of DMF/water (10 mL, 1/4, v/v) containing
162 88 mg OVA within 30 min. Under the constant conditions, the reaction was maintained for
163 another 6 h. The subsequent procedures were identical to that of T-BSA described above.

164 Hapten-protein conjugates, T-BSA and T-OVA, were characterized by SDS-PAGE, and
165 UV spectra. SDS-PAGE analysis of conjugates was performed by a 3% stacking gel and a

166 10% separating gel with Coomassie blue staining. UV spectra were obtained by spectral
167 scanning (240-320 nm) of the proteins and their conjugates with a UV-3310
168 spectrophotometer (Hitachi, Japan).

169 **Preparation of Polyclonal Antibody.** Female BALB/c mice were obtained from the
170 Experimental Animal Research Center, Fourth Military Medical University (Shaanxi,
171 China), with an average body weight of 20 g. They were housed under standard laboratory
172 conditions with free access to drinking water and a commercial pellet diet. Animal
173 manipulations were carried out in compliance with the Animal Management Rules of the
174 Ministry of Health of China (No. 55, 2001). Six female BALB/c mice of 6 weeks old were
175 immunized with antigen following the immunizing protocol described by Leenaars and
176 Hendriksen[39]. Before immunization, blood was collected by tail bleeding to prepare control
177 serum. Initial immunization was carried out by multiple subcutaneous injections with an
178 emulsion of physiological brine solution containing 50 μg of T-BSA and complete Freund's
179 adjuvant (1/1, v/v) for each mouse. Two weeks later, animals were boosted with 50 μg of
180 T-BSA in incomplete Freund's adjuvant per mouse for two times at one week intervals.
181 One week after the third inoculation, each mouse was given a single intraperitoneal
182 injection with 100 μg of T-BSA in a physiological brine solution. After one week, the
183 blood samples were harvested by removing the eyeballs and titers of antisera were
184 monitored by indirect enzyme-linked immunosorbent assays (ELISAs) described by
185 Manclús and Montoya[40] to evaluate the immune responses. Antiserum with highest titer
186 was purified by affinity column chromatography on Sepharose-4B gel to prepare
187 polyclonal antibody. Antiserum titer was defined as the reciprocal of the highest dilution

188 which gave an absorbance of about 1.0. The concentration of the purified polyclonal
189 antibody was measured using a NanoVue Plus at 280 nm, and the sample was stored at
190 −20°C for further use.

191 **Antifungal Bioassay.** The antifungal activity of TTY against Ggt was determined by the
192 agar dilution method described by Rios et al.[41] Stocks of carabrone and TTY in DMSO
193 with different concentrations were prepared in advance. Stock solutions (50 μL) were
194 added to molten PDA (50 mL) at low temperature (45-50°C), respectively. After sufficient
195 mixing, the solutions were poured into 90-mm petri dishes immediately to a thickness of
196 2-3 mm, with different concentrations of carabrone or TTY (6.25, 12.50, 25.00, 50.00, and
197 100.00 μg/mL). PDA supplemented with DMSO served as the control. After plating, a
198 4-mm diameter mycelial disc from the actively growing colony front was then placed with
199 the inoculum side down in the center of each treatment plate, aseptically. Plates were then
200 incubated in the dark at a constant temperature of 25°C for 7 days. All experiments were
201 conducted in a sterile environment and performed in triplicate. Mean growth values were
202 measured and subsequently converted into an inhibition rate of mycelial growth in relation
203 to control treatment according to the following formula:

204 $$\text{Inhibition rate (\%)} = [(M_c - M_t)/ (M_c - 0.4)] \times 100$$

205 where M_c and M_t represent the mycelial growth diameter of control and treatment group,
206 respectively. The EC_{50} values (effective dose for 50% inhibition) were calculated
207 statistically by probit analysis using the probit package of SPSS 23.0 software (SPSS Inc.,
208 USA).

209 **Effects of Carabrone on Hyphal Morphology and Ultrastructure**. The effects of
210 carabrone on hyphal morphology and ultrastructure were investigated using the reported
211 method of Shao et al.[42] A prepared mycelial agar disc from a 5-day-old culture was
212 inoculated in the center of PDA plate with EC_{50} value (28.45 μg/mL) of carabrone and
213 incubated at 25°C for 7 days in dark. PDA plates without carabrone treatment were used as
214 the control.

215 For scanning electron microscope (SEM) observation, mycelial discs (3 mm × 5 mm × 5
216 mm) were fixed with 2.5% glutaraldehyde in 0.1 M phosphate buffer (pH 7.2) overnight at
217 4°C. After fixation, mycelial discs were gently washed with 0.1 M phosphate buffer (pH
218 7.2) for 6 times (15 min each). Then, the fixed samples were dehydrated in a graded
219 ethanol series (once at 30, 50, 70, 80, 90% and three times at 100%, v/v) for 15 min in each.
220 After the dehydration period, each specimen was dipped into pure isoamyl acetate for
221 replacement two times, each for 30 min. At last, the samples were dried by supercritical
222 carbon dioxide, gold-coated by a E1010 sputter coating machine (Hitachi, Japan) for 60 s,
223 and then imaged using a JSM-6360LV SEM (JEOL, Japan). No treated mycelial discs were
224 as the control.

225 For transmission electron microscopy (TEM) observation, the fixed mycelia for SEM
226 were post-fixed with 1% osmic acid for 2 h. Then, the samples were fully washed with 0.1
227 M phosphate buffer (pH 7.2) immediately followed by dehydration as described above.
228 Samples were dipped into epoxy propane two times (15 min each). After that, the
229 specimens were passed through the solution of epoxy resin and epoxy propane (1:1, v/v)
230 for 1 h and embedded in epoxy media at 55°C for 48 h. The ultrathin sections were

231 prepared with a Ultramicrotome (Leica-ULTRACUT, Germany), contrasted with 2%
232 uranyl acetate followed by 2% lead citrate, and examined on a JEM-1230 TEM (Hitachi,
233 Japan). At least three samples from the treated and control group were examined by TEM
234 and SEM, respectively.

235 **Effect of Carabrone on the Mitochondrial concentration.** The extraction of
236 mitochondria was according to the reported method by Tamura et.al. with some
237 modifications.[43] Fifteen prepared mycelial agar discs (4 mm) from a 7-day-old culture
238 were inoculated in 100 mL potato dextrose broth (potato infusion from 200 g/L, 20 g/L
239 dextrose) with EC_{50} (28.45 μg/mL) or EC_{70} (49.97 μg/mL) value of carabrone and
240 incubated at 25°C with 180 rpm for 7 days in dark. Mycelia were harvested through
241 filtration by sterile gauze and washed three times using 0.7% NaCl isotonic solution. After
242 freeze-drying for 24 h, a certain quality of mycelium cells was grinded in liquid nitrogen
243 and the obtained powder was then resuspended in a five-fold volume of pre-cooling
244 extraction buffer (10 mM KCl, 5 mM EDTA, 250 mM sucrose, 1.5 mg/mL BSA, 20 mM
245 HEPES-Tris pH 7.2) for homogenization. The homogenate was centrifuged (1,500 rpm, 10
246 min, 4°C), and the supernatant was retained. The precipitate obtained was resuspended in
247 the same volume of extraction buffer and recentrifuged under the above conditions. The
248 supernatant was combined and centrifuged at 4°C (10,000 rpm, 20 min). The resulting
249 precipitate was washed with the extraction buffer without BSA. The final mitochondrial
250 fraction was suspended in a small volume of a cold buffer solution (250 mM sucrose, 20
251 mM HEPES-Tris, pH 7.2) as the mitochondrial sample. All experiments were performed in
252 triplicate. The protein level of a mitochondrial sample was detected by the coomassie

253 brilliant blue G-250 dye-binding method[44] and used as the marker of the mitochondrial
254 concentration[45].

255 **Absorption Kinetics of TTY in Mycelial Cells.** TTY was dissolved in an aqueous
256 solution (0.2% DMSO) to prepare the work solutions with different concentrations (0.3,
257 0.35, 0.4, and 0.8 μM). Mycelial cells were inoculated in potato-dextrose broth and
258 cultivated in darkness at 25°C on an Eberbach rotary shaker at 150 rpm for 72 h.

259 For absorption kinetics study, the prepared mycelia were washed three times with
260 ultrapure water and then surface water was removed by a filter paper. Mycelial cells (10
261 mg, wet weight) were placed on a glass slide and stained with the ready solution of TTY
262 (20 μL) in the dark at room temperature for a designated time period (5, 10, 15, 30, 60, 90,
263 120, 150, 180, 210, and 240 min). After fully washing, the samples were observed with a
264 structured illumination microscopy (Observer Zl, Zeiss, Germany) excited at 365 nm with
265 the emission wavelength of 445 nm. No-TTY treated sample was as control. Fluorescence
266 intensity per unit area of 90 hyphae in one visual field was counted by an Image J software
267 package and three visual fields were randomly selected for each treatment.

268 **Stability of TTY in Mycelial Cells.** Mycelial cells (500 mg, wet weight) were stained
269 with a TTY work sloution (1 mL, 0.4 μM) in the dark at room temperature for 90 min.
270 After staining, the stained mycelial cells were fully washed to remove the free TTY and
271 then were kept under the same conditions for another 2 h. The obtained mycelial cells were
272 collected and grinded in liquid nitrogen. The sample was then extracted with methanol (2
273 mL, chromatographic grade) and centrifuged at 4°C (8,000 rpm, 5 min). The supernatant
274 was filtered by a millipore filter (0.22 μm) for LC-HRMS analysis. Mycelial cells without

275 TTY treatment were used as the control. The LC-HRMS analysis was performed on an AB
276 Sciex Triple TOF 5600+ System (USA) using a methanol-water elution system (0-5 min,
277 10 vol% methanol in water; 5-10 min, 10 to 40% methanol; 10-15 min, 40 to 70%
278 methanol; 15-20 min, 70 to 90% methanol; and 20-25 min, 90 to 100% methanol). A C_{18}
279 reversed-phase column was used for separation. The injection volume was 10 μL, and the
280 flow rate was 1 mL/min.

281 **Cell imaging.** Stocks of carabrone (0.1 mM), TTY (0.4 mM), MitoTrackerR Green FM
282 (1 mM), and MitoTrackerR Red CMXRos (1 mM) were freshly prepared using DMSO as
283 solvent and diluted with ultrapure water before use. All the dyeing processes in this paper
284 were operated under dark condition. The Pearson's colocalization coefficient was
285 calculated using a Colocalization Finder plugin of a free image processing software Image
286 J. The software and plugin are available on the website (https://imagej.nih.gov/ij/).

287 For FC imaging, mycelial cells (10 mg, wet weight) were washed three times with
288 ultrapure water, and then incubated with a mixture solution containing 0.4 μM TTY and
289 100 nM MitoTrackerR Green FM at room temperature for 1 h. After rinsing with ultrapure
290 water to remove the free dyes, mycelial cells were re-dyed with RedDot™1 (1:200 dilution)
291 under a constant condition (30°C, 1 h). After fully washing, the sample was observed with
292 a structured illumination microscopy (Observer Zl, Zeiss, Germany) directly. TTY was
293 excited at 365 nm with the emission wavelength of 445 nm. Mitochondrial probe,
294 MitoTrackerR Green FM, was excited at 470 nm with the emission wavelength of 525 nm.
295 Excitation of RedDot™1 was carried out using 640 nm and the emission wavelength was
296 690 nm. Photos were collected using a Axio Visio Release 4.8.2 SP3 software.

297 For IF imaging, mycelial cells prepared were first incubated with a carabrone solution
298 (0.1 μM) at 25°C for 12 h. Then, the sample was washed with ultrapure water for three
299 times to drain off the free carabrone. After staining with MitoTrackerR Red CMXRos (100
300 nM) at 25°C for 2 h, mycelial cells were fixed with 2% paraformaldehyde for 40 min and
301 the fixed cells were rinsed three times with MSB (PIPES, 50 mM; EGTA, 2 mM, $MgSO_4$,
302 2 mM; pH 6.9) at 5 min intervels. The sample was then added to a mixed enzyme solution
303 (Cellulase/Driselase/Lyticase) for 5 min in the dark. After enzymolysis, the mycelial cells
304 were washed with PBS (10 mM, pH 7.2) for three times every 5 min and blocked in PBS
305 supplemented with BSA (5 mg/mL) for 30 min in the dark. The sample was stained
306 successively with primary antibody (1:1000 dilution in PBS, 37°C, 1 h), Anti-Mouse IgG
307 (whole molecule)-FITC (1:100 dilution in PBS, 37°C, 1 h), and washed with PBS as above
308 following each staining period. After immunofluorescence staining, the sample imaging
309 was performed on a confocal laser scanning microscopy equipped with Leica application
310 suite sdvanced fluorescence software (Leica TCS SP8, Germany) directly. MitoTrackerR
311 Red CMXRos: excitation wavelength, 561 nm; emission spectrum, 630 - 660 nm.
312 Anti-Mouse IgG (whole molecule)-FITC: excitation wavelength, 488 nm; emission
313 spectrum, 520 - 550 nm.

314 **RESULTS AND DISCUSSION**

315 **Synthesis and Characterization.** *TTY*. For fluorescence localization analysis, a
316 fluorescent carabrone conjugate, TTY, was designed and synthesized according to the
317 synthetic route illustrated in Scheme 1. *N*-methyl anthranilic acid (TY) was chosen as the
318 fluorogen, the carboxyl group of which was first activated by NSH to obtain *N*-methyl

319 anthranilic acid succinimidyl ester (1).[35] Compound **1** was further modified by
320 ethylenediamine to give *N*-(2-aminoethyl)-2-(methylamino)benzamide (HH2).[36]
321 Meanwhile, carboxylated carabrone derivative, HH1, was prepared through the imidization
322 of carabrone with carboxymethoxylamine hydrochloride using sodium acetate as catalyst
323 under a nitrogen atmosphere.[34] TTY was finally obtained through the condensation
324 reaction between HH1 and HH2, in the presence of EDC as coupling reagent and DMAP
325 as catalyst under mild conditions. The structures of the newly synthesized compounds were
326 characterized correctly by ^{1}H NMR, ^{13}C NMR, and ESI-MS (Figure S1-S6). Moreover,
327 fluorescence spectrophotometer was also employed to investigate the fluorescent properties
328 of compound TTY with results shown in Figure S7. TTY exhibited excitation and emission
329 spectra maximum peaks at 381 nm ($\lambda_{ex, max}$) and 445 nm ($\lambda_{em, max}$) in methanol, respectively.
330 *Hapten-protein conjugates.* As outlined in Scheme 1, immunogen (T-BSA) was prepared
331 by the active ester method[37], using HH1 as the hapten and BSA as the carrier for
332 polyclonal antibody production. Meanwhile, Coating antigen (T-OVA) was synthesized
333 through coupling of HH1 with OVA by the mixed anhydride method[38] for indirect ELISAs.
334 SDS-PAGE was used for mobility shift detection of hapten-protein conjugates and the
335 results were shown in Figure S8. From SDS-PAGE, the bands of T-BSA and T-OVA
336 appeared at higher molecular weight positions with slower mobility relative to their
337 unreacted proteins, indicating successful protein conjugation.
338 The ultraviolet-visible spectral changes of hapten-protein conjugates were also
339 monitored to confirm with their identities by UV spectroscopy. As shown in Figure S9,
340 T-BSA exhibited a 10-nm blue shift from 278 nm to 268 nm relative to BSA, and T-OVA a

341 7-nm blue shift from 278 nm to 270 nm relative to OVA under the same conditions,
342 verifying that HH1 was successfully attached to the carrier proteins.

343 **Production of Polyclonal Antibody.** Antigen design plays a key role in polyclonal
344 antibody production. Due to weak antigenicity of carabrone with low molecular weight, it
345 must be coupled to a carrier protein to elicit an immune response.[46] In order to generate
346 antibody with high sensitivity and specificity, the binding strategy was also designed
347 cautiously to ensure the minimum conformational changes of hapten relative to the targeted
348 analyte even after conjugation with the carrier protein.[47] Moreover, previous study revealed
349 that antibodies produced by single antigens might have higher affinities to the targets.[37]
350 Based on these information, HH1 retaining the core structure of carabrone was selected as
351 the hapten, and its BSA conjugate as the immunogen. After four rounds of immunization
352 with single T-BSA, polyclonal antisera produced by six female BALB/c mice were isolated
353 and their titers against carabrone were tested by indirect ELISAs (Table S1). Antisera
354 (TPAbs 1-6) exhibited different affinities to the coating antigen (T-OVA) with titers ranging
355 from 64,000 to 256,000, which were higher than those of previously reported antisera
356 against various pesticides.[48] TPAbs-4 with the highest titer (256,000) was selected for
357 antibody purification. The concentration of the purified polyclonal antibody was about 4.52
358 mg/mL.

359 **Antifungal Activity.** Physicochemical properties of a parent compound will be
360 inevitably changed if it is modified with a fluorogen, including molecular weight, the
361 octanol/water partitioning coefficient value, etc., which may even affect its combination
362 with the target consequently. Previous studies of our group showed that carabone

363 derivatives modified at C-4 position exhibited diverse antifungal activities against *Botrytis*
364 *cinereal* and *Colletotrichum lagenarium* through altering their affinities to the unclear
365 target of carabrone.[49, 50] Thus, to investigate the effect of substituent fluorogen on the
366 recognition of carabrone to its target, the effects of TTY and carabrone on the mycelial
367 growth of Ggt were evaluated *in vitro*. As illustrated in Table 1, TTY performed similar
368 EC_{50} value (33.68 μg/mL) to that of carabrone (28.45 μg/mL), verifying that TTY still
369 maintains the capacity of selectively binding to the target of carabrone. Thus, the
370 fluorescent conjugate (TY) does not affect the biological activity of carabrone.

371 **Absorption Kinetics of TTY.** To determine the potential of TTY to be used as a
372 fluorescent subcellular tracer, the absorption behavior of TTY was examined by
373 monitoring fluorescence intensity of mycelia stained with different concentrations of TTY
374 (0.3, 0.35, 0.4, and 0.8 μM) over various time periods (0-240 min). As depicted in Figure 2,
375 TTY absorption exhibited a time- and dose-dependent manner. Adsorption equilibrium was
376 reached after 90 min and a saturated absorption was reached when the concentration of
377 TTY was over 0.4 μM. We thus used the optimized staining condition (0.4 μM TTY,
378 dyeing time: 90 min) for localization experiment. Under the optimal conditions obtained, a
379 fluorescence image with evident subcellular distribution was represented (Figure S10),
380 which indicated that TTY could enter the mycelial cells of Ggt for cell imaging.

381 **Stability of TTY in Mycelial Cells.** An ideal fluorescent tracer should be stable
382 throughout the imaging period**.** Thus, the TTY present in the mycelial cells at 2 h was
383 identified by LC-HRMS analysis. As shown in Figure S11, the chromatographic peak for
384 compound TTY (*m/z*, $[M + H]^+$ 497.2751, and $[M + Na]^+$ 519.2583) was found at 14.18

385 min while no identical chromatographic peak of TTY was found in the control group
386 (Figure S12). Moreover, we have searched the possible decomposed products of TTY
387 (Figure S14) in the TOF MS spectrum from 6 min to 25 min using an Analyst TF 1.7.1
388 Software and there were no matched MS peaks for these products (Figure S13). Therefore,
389 TTY was relatively stable during the experimental period. These findings indicate that
390 TTY is a suitable fluorescent surrogate of carabrone and is believed to be capable of
391 revealing the subcellular localization of carabrone within Ggt.

392 **Hyphal Morphology and Ultrastructure.** Previous work of our group showed that
393 carabrone possessed a remarkable inhibitory effect against the mycelial growth of Ggt.[17]
394 To gain more evidence about the mode of antifungal action of carabrone treatment, the
395 hyphal morphology of Ggt was observed by SEM with results shown in Figure 3. The
396 control sample exhibited a normal morphology with uniform, smooth, uniseriate, and
397 robust hyphae with plump growing points (Figure 3a). The carabrone treated sample,
398 however, showed altered morphology characterized by twisted and irregular hyphae with
399 slight deformity at the growing points (Figure 3b) and even cellular collapse (Figure 3c).

400 TEM was employed to study the ultrastructural alterations of Ggt when treated with
401 carabrone and the results were illustrated in Figure 4. A typical fungal ultrastructure of
402 intact cell wall with normal thickness, regular and smooth cell membrane, evenly
403 distributed cellular cytoplasm, and regularly shaped organelles in the mycelia is clearly
404 represented by TEM images of the control treatment (Figure 4a, b). For the carabrone
405 treatment with EC_{50} value, no evident changes were viewed in the structures of cell wall,
406 cell membrane and the diaphragm of the mycelia. Interestingly, mitochondrial abnormality

407 was observed in the treated mycelia which could be described as (i) the hazy outline of
408 mitochondria (Figure 4c), (ii) medullary transition of mitochondria (Figure 4d), (iii) excess
409 accumulation of unclear settlings in mitochondria (Figure 4e), and (iv) vacuolar
410 degeneration of mitochondria (Figure 4f). These findings suggested that the mitochondria
411 of Ggt might correlated with the action mechanism of carabrone.

412 **Mitochondrial Concentration.** To validate our ultrastructural findings, we sought to
413 test the changes of mitochondrial concentration of Ggt treated with carabrone. The effect
414 of carabrone on the mitochondrial concentration was evaluated by testing the protein
415 content of mitochondria (Table 2).[45] After exposure to carabrone for 7 days, the
416 mitochondrial concentration of Ggt decreased evidently ($P < 0.05$) along with the
417 increasing concentration of carabrone (EC_{50}, 28.45 μg/mL; EC_{70}, 49.97 μg/mL), in
418 agreement with the alterations of mitochondrial structure.

419 **Subcellular Imaging.** Given the fact that the aforementioned effects of carabrone on
420 Ggt (e.g. ultrastructural alterations, decreases in mitochondrial concentration) are closely
421 related to mitochondria, two imaging techniques (FC and IF) were employed to validate
422 the mitochondrial targeting of carabrone.

423 For FC imaging, three dyes with distinctive emission wavelengths (TTY, 445 nm;
424 MitoTrackerR Green FM, 525 nm; RedDot™1, 690 nm) were utilized. As depicted in
425 Figure 5, S15, TTY and MitoTrackerR Green FM (a mitochondrial dye) overlapped
426 perfectly while no overlay was observed between TTY and RedDot™ (a commercial
427 nuclear probe). Pearson's colocalization coefficient,[51, 52] describing the correlation of the
428 intensity distribution between TTY and MitoTrackerR Green FM signal, was 0.83 (Figure

429 5h). Thus, FC imaging strongly supports the mitochondrial localization of carabrone.

430 For IF imaging, polyclonal antibody specific to carabrone was used as the primary
431 antibody to recognize intracellular carabrone, and FITC labeled Anti-Mouse IgG (whole
432 molecule) as the secondary antibody. Meanwhile, a commercially available dye,
433 MitoTrackerR Red CMXRos was employed for colocalization study. Again, excellent
434 colocalization between Anti-Mouse IgG (whole molecule)-FITC and the MitoTrackerR
435 Red CMXRos was observed (Figure 6, S16), with the Pearson's colocalization coefficient
436 being 0.86 (Figure 6f). These results suggested that carabrone was predominantly present
437 in the mitochondria.

438 α,β-unsaturated lactones, such as britannin,[20] arucanolide,[21] parthenolide,[22]
439 costunolide,[23] and isocostunolide[24] exert their biologic functions via mitochondria-related
440 pathways. Our previous study showed that carabrone could inhibit the intracellular
441 oxidation process in Ggt, and exert some impacts on the mitochondria, such as vacuolar
442 degeneration,[25] which was consistent with the results obtained in this study. Additionally,
443 when treated with carabrone, the activity of respiratory chain complexes I-V was
444 determined to be significantly decreased, especially that of the complex III, and the
445 expression levels of the associated genes were up-regulated except *GgCyc1*,[26]
446 demonstrating that carabrone involved in the respiratory electron transfer pathway either
447 directly or indirectly in Ggt. In this paper, we confirmed not only the effects of carabrone
448 on the mitochondrial structure and concentration, but also its mitochondrial targeting using
449 FC and IF imaging techniques. The excessive accumulation of reactive oxygen species
450 (ROS) in the mitochondria was also observed in Ggt when treated with carabrone (data not

published). These results indicate that carabrone selectively distributes in the mitochondria of Ggt and functions on the respiratory electron-transport chain, especially the complex III, which leads to ROS increase and the death of mycelial cells followed. However, the detailed pathway of action on mitochondria is still unclear, and a further study of mitochondria-related pathway induced by carabrone in Ggt is in progress.

In conclusion, the major effects of carabrone as a potential botanical antifungal agent against Ggt were the variations in mitochondrial structure and the decreased concentration. A fluorescent conjugate of carabrone, TTY, was well designed and first obtained via covalent coupling of a smart fluorophore with a soft linker. Antifungal activity and absorption kinetics indicated that TTY was a reasonable fluorescent surrogate of carabrone and suitable to reveal the subcellular distribution of carabrone analogues. Polyclonal antibody specific to carabrone was also successfully prepared by immunizing mice with a well-designed immunogen according to a standard protocol. Subcellular imaging with FC and IF provided identical and adequate evidences that the actual site(s) of action of carabrone lay in the mitochondria of Ggt, orienting our follow-up study for elucidating the detailed mechanism of carabrone against Ggt. More importantly, the strategies established for subcellular localization study of a natural substance in this paper could be also applied in exploring the action mechanism of other drugs.

AUTHOR INFORMATION

Corresponding Author

*(Juntao Feng) Fax: +86-029-87092122. E-mail: fengjt@nwafu.edu.cn.

Funding

473 This work was financially supported by the National Natural Science Foundation of China
474 (No. 31272074).

475 **Notes**

476 The authors declare no competing financial interest.

477 **REFERENCES**

478 (1) Gutteridge, R. J.; Bateman, G. L.; Todd, A. D. Variation in the effects of take□all disease on grain
479 yield and quality of winter cereals in field experiments. *Pest Manag. Sci.* **2003**, *59*, 215-224.

480 (2) Keenan, S.; Cromey, M.; Harrow, S.; Bithell, S.; Butler, R.; Beard, S.; Pitman, A. Quantitative PCR
481 to detect *Gaeumannomyces graminis* var. *tritici* in symptomatic and non-symptomatic wheat roots.
482 *Australas. Plant Path.* **2015**, *44*, 591-597.

483 (3) Yang, M. M.; Mavrodi, D. V.; Mavrodi, O. V.; Bonsall, R. F.; Parejko, J. A.; Paulitz, T. C.;
484 Thomashow, L. S.; Yang, H. T.; Weller, D. M.; Guo, J. H. Biological control of take-all by fluorescent
485 *Pseudomonas spp.* from Chinese wheat fields. *Phytopathology* **2011**, *101*, 1481-1491.

486 (4) Kwak, Y.-S.; Bakker, P. A.; Glandorf, D. C.; Rice, J. T.; Paulitz, T. C.; Weller, D. M. Diversity,
487 virulence, and 2, 4-diacetylphloroglucinol sensitivity of *Gaeumannomyces graminis* var. *tritici* isolates
488 from Washington State. *Phytopathology* **2009**, *99*, 472-479.

489 (5) Lei, P.; Zhang, X. B.; Xu, Y.; Xu, G. F.; Liu, X. L.; Yang, X. L.; Zhang, X.; Ling, Y. Synthesis and
490 fungicidal activity of pyrazole derivatives containing 1, 2, 3, 4-tetrahydroquinoline. *Chem. Cent. J.* **2016**,
491 *10*, 40.

492 (6) Pérez-García, A.; Romero, D.; De Vicente, A. Plant protection and growth stimulation by
493 microorganisms: biotechnological applications of *Bacilli* in agriculture. *Curr. Opin. Biotechnol.* **2011**,
494 *22*, 187-193.

(7) Yoon, M. Y.; Cha, B.; Kim, J. C. Recent trends in studies on botanical fungicides in agriculture. *Curr. Opin. Biotechnol.* **2013**, *29*, 1-9.

(8) Cook, R. J. Take-all of wheat. Physiol. *Mol. Plant Pathol*. **2003**, *62*, 73-86.

(9) Kwak, Y. S.; Weller, D. M. Take-all of wheat and natural disease suppression: a review. *Plant Pathol. J.* **2013**, *29*, 125.

(10) Liu, B.; Qiao, H. P.; Huang, L. L.; Buchenauer, H.; Han, Q. M.; Kang, Z. S.; Gong, Y. F. Biological control of Take-all in wheat by endophytic *Bacillus Subtilis* E1r-J and potential mode of action. *Biol. Control* **2009**, *49*, 277-285.

(11) Yang, L. R.; Quan, X.; Xue, B. G.; Goodwin, P. H.; Lu, S. B.; Wang, J. H.; Du, W.; Wu, C. Isolation and identification of *Bacillus subtilis* strain YB-05 and its antifungal substances showing antagonism against *Gaeumannomyces graminis* var. *tritici*. *Biol. Control* **2015**, *85*, 52-58.

(12) Gong, L.; Tan, H. B.; Chen, F.; Li, T. T.; Zhu, J. Y.; Jian, Q. J.; Yuan, D. B.; Xu, L. X.; Hu, W. Z.; Jiang, Y. M.; Duan, X. W. Novel synthesized 2, 4-DAPG analogues: antifungal activity, mechanism and toxicology. *Sci. Rep*. **2016**, *6*.

(13) Feng, J. T.; Ma, Z. Q.; Li, J. H.; He, J.; Xu, H.; Zhang, X. Synthesis and antifungal activity of carabrone derivatives. *Molecules* **2010**, *15*, 6485-6492.

(14) Maruyama, M.; Omura, S. Carpesiolin from Carpesium abrotanoides. *Phytochemistry* **1977**, *16*, 782-783.

(15) Yang, C.; Shi, Y. P.; Jia, Z. J. Sesquiterpene lactone glycosides, eudesmanolides, and other constituents from *Carpesium Macrocephalum*. *Planta Med.* **2002**, *68*, 626-630.

(16) Jiang, J. W., Manuscript of Active Ingredients of Vegetable Drug. People's Health Press Beijing, China: 1986.

517 (17) Han, X. S.; Xu, D.; Feng, J. T.; Zhang, X. Fungicidal activity of carabrone. *J. Northwest A&F Univ.*
518 **2014**, *42*, 178-184.
519 (18) Zhang, S. Y.; Won, Y. K.; Ong, C. N.; Shen, H. M. Anti-cancer potential of sesquiterpene lactones:
520 bioactivity and molecular mechanisms. *Curr. Med. Chem. Anticancer Agents.* **2005**, *5*, 239-249.
521 (19) Kitson, R. R.; Millemaggi, A.; Taylor, R. J. The Renaissance of α□Methylene□γ□butyrolactones:
522 New Synthetic Approaches. *Angew. Chem. Int. Ed.* **2009**, *48*, 9426-9451.
523 (20) Hamzeloo-Moghadam, M.; Aghaei, M.; Fallahian, F.; Jafari, S. M.; Dolati, M.; Abdolmohammadi,
524 M. H.; Hajiahmadi, S.; Esmaeili, S. Britannin, a sesquiterpene lactone, inhibits proliferation and induces
525 apoptosis through the mitochondrial signaling pathway in human breast cancer cells. *Tumor Biol.* **2015**,
526 *36*, 1-8.
527 (21) Nakagawa, Y.; Iinuma, M.; Matsuura, N.; Yi, K.; Naoi, M.; Nakayama, T.; Nozawa, Y.; Akao, Y. A
528 potent apoptosis-inducing activity of a sesquiterpene lactone, arucanolide, in HL60 cells: a crucial role
529 of apoptosis-inducing factor. *J. Pharmacol. Sci.* **2005**, *97*, 242.
530 (22) Zhang, S.; Ong, C. N.; Shen, H. M. Involvement of proapoptotic Bcl-2 family members in
531 parthenolide-induced mitochondrial dysfunction and apoptosis. *Cancer Lett.* **2004**, *211*, 175-188.
532 (23) Lee, M.-G.; Lee, K.-T.; Chi, S.-G.; PARK, J.-H. Costunolide induces apoptosis by ROS-mediated
533 mitochondrial permeability transition and cytochrome C release. *Biol. Pharm. Bull.* **2001**, *24*, 303-306.
534 (24) Chen, C. N.; Huang, H. H.; Wu, C. L.; Lin, C. P.; Hsu, J. T.; Hsieh, H. P.; Chuang, S. E.; Lai, G.
535 M. Isocostunolide, a sesquiterpene lactone, induces mitochondrial membrane depolarization and
536 caspase-dependent apoptosis in human melanoma cells. *Cancer Lett.* **2007**, *246*, 237.
537 (25) Wang, Y. M. Effects of Carabrone on Five plant diseases and the growth and development of
538 *Gaeumannomyces Graminis* Var. *Tritici*. Northwest A & F University, Yangling, 2009.

539 (26) Wang, M.; Wang, L. Y.; Han, L. R.; Zhang, X.; Feng, J. T. The effect of carabrone on
540 mitochondrial respiratory chain complexes in *Gaeumannomyces Graminis*. *J. Appl. Microbiol.* **2017**,
541 *123*, 1100-1110.
542 (27) Stadler, C.; Rexhepaj, E.; Singan, V. R.; Murphy, R. F.; Pepperkok, R.; Uhlén, M.; Simpson, J. C.;
543 Lundberg, E. Immunofluorescence and fluorescent-protein tagging show high correlation for protein
544 localization in mammalian cells. *Nat. Methods* **2013**, *10*, 315-323.
545 (28) Gonzalez, A. A.; Prieto, M. C. Roles of collecting duct renin and (pro) renin receptor in
546 hypertension: mini review. *Ther. Adv. Cardiovasc. Dis.* **2015**, *9*,191-200.
547 (29) Thurber, G. M.; Yang, K. S.; Reiner, T.; Kohler, R. H.; Sorger, P.; Mitchison, T.; Weissleder, R.
548 Single-cell and subcellular pharmacokinetic imaging allows insight into drug action *in vivo*. *Nat.*
549 *Commun.***2013**, *4*, 1504.
550 (30) Vinegoni, C.; Dubach, J. M.; Thurber, G. M.; Miller, M. A.; Mazitschek, R.; Weissleder, R.
551 Advances in measuring single-cell pharmacology *in vivo*. *Drug Discov. Today* **2015**, *20*, 1087-1092.
552 (31) Irani, N. G.; Di Rubbo, S.; Mylle, E.; Van den Begin, J.; Schneider-Pizoń, J.; Hniliková, J.; Šíša,
553 M.; Buyst, D.; Vilarrasa-Blasi, J.; Szatmári, A.-M. Fluorescent castasterone reveals BRI1 signaling from
554 the plasma membrane. *Nat. Chem. Biol.* **2012**, *8*, 583-589.
555 (32) Wang, J.; Lei, Z. W. ; Wen, Y. J. ; Mao, G. L. ; Wu, H. X. ; Xu, H. H. A novel fluorescent
556 conjugate applicable to visualize the translocation of glucose-fipronil. *J. Agric. Food. Chem.* **2014**, *62*,
557 8791-8798.
558 (33) Kang, C. K.; Yamada, K.; Usuki, Y.; Ogita, A.; Fujita, K. I.; Tanaka, T. Visualization analysis of
559 the vacuole-targeting fungicidal activity of amphotericin B against the parent strain and an
560 ergosterol-less mutant of Saccharomyces cerevisiae. *Microbiology* **2013**, *159*, 939-947.

561 (34) Boivin, J.; Fouquet, E.; Schiano, A. M.; Zard, S. Z. Iminyl radicals: Part III. Further synthetically
562 useful sources of iminyl radicals. *Tetrahedron* **1994**, *50*, 1769-1776.
563 (35) Gavande, N.; Kim, H. L.; Doddareddy, M.; Johnston, G. A. R.; Chebib, M.; Hanrahan, J. R.
564 Design, Synthesis, and Pharmacological Evaluationof Fluorescent and Biotinylated Antagonists of ρ1
565 GABAC Receptors. *Acs Med.Chem. Lett.* **2013**, *4*, 402-407.
566 (36) Leung, A. H.; Jin, J. F.; Wang, S. X.; Lei, H.; Wong, W. T. Inflammation targeted Gd(3+)-based
567 MRI contrast agents imaging tumor and rheumatoid arthritis models. *Bioconjugate Chem.* **2014**, *25*,
568 1112-1123.
569 (37) Shi, H. Y.; Li, H. X.; Hua, X. D.; Zheng, Z. T.; Zhu, G. N.; Wang, M. H. Characterization of
570 Multihapten Antigens on Antibody Sensitivity and Specificity for Parathion. *Anal. Lett.* **2014**, *47*,
571 2699-2707.
572 (38) Gendloff, E. H.; Casale, W. L.; Ram, B. P.; Tai, J. H.; Pestka, J. J.; Hart, L. P. Hapten-protein
573 conjugates prepared by the mixed anhydride method : Cross-reactive antibodies in heterologous antisera.
574 *J. Immunol. Methods* **1986**, *92*, 15.
575 (39) Leenaars, M.; Hendriksen, C. F. Critical steps in the production of polyclonal and monoclonal
576 antibodies: evaluation and recommendations. *Ilar J.* **2005**, *46*, 269-279.
577 (40) Manclús, J. J.; Montoya, A. Development of immunoassays for the analysis of chlorpyrifos and its
578 major metabolite 3,5,6-trichloro-2-pyridinol in the aquatic environment. *Anal. Chim. Acta* **1995**, *311*,
579 341-348.
580 (41) Rios, J. L.; Recio, M. C.; Villar, A. Screening methods for natural products with antimicrobial
581 activity: A review of the literature. *J. Ethnopharmacol.* **1988**, *23*, 127-149.
582 (42) Shao, X.; Cheng, S.; Wang, H.; Yu, D.; Mungai, C. The possible mechanism of antifungal action

583 of tea tree oil on *Botrytis cinerea*. *J. Appl. Microbiol.* **2013**, *114*, 1642-1649.

584 (43) Tamura, H.; Mizutani, A.; Yukioka, H.; Miki, N.; Ohba, K.; Masuko, M. Effect of the
585 methoxyiminoacetamide fungicide, SSF129, on respiratory activity in *Botrytis*. *Pestic. Sci.* **1999**, *55*,
586 681-686.

587 (44) Grintzalis, K.; Georgiou, C. D.; Schneider, Y. J. An accurate and sensitive Coomassie Brilliant
588 Blue G-250-based assay for protein determination. *Anal. Biochem.* **2015**, *480*, 28-30.

589 (45) Frezza, C.; Cipolat, S.; Scorrano, L. Organelle isolation: functional mitochondria from mouse
590 liver, muscle and cultured fibroblasts. *Nat. Protoc.* **2007**, *2*, 287.

591 (46) Hertzog, P. J.; Shaw, A.; Smith, J. R. L.; Garner, R. C. Improved conditions for the production of
592 monoclonal antibodies to carcinogen-modified DNA, for use in enzyme-linked immunosorbent assays
593 (ELISA). *J. Immunol. Methods* **1983**, *62*, 49-58.

594 (47) Spinks, C. A. Broad-specificity immunoassay of low molecular weight food contaminants: new
595 paths to Utopia. *Trends Food Sci. Tech.* **2000**, *11*, 210-217.

596 (48) Liu, R.; Liu, Y.; Lan, M. J.; Taheri, N.; Cheng, J. L.; Guo, Y. R.; Zhu, G. N. Evaluation of a
597 water-soluble adjuvant for the development of monoclonal antibodies against small-molecule
598 compounds. *J. Zhejiang Univ. Sci. B* **2016**, *17*, 282-293.

599 (49) Feng, J. T.; Wang, H.; Ren, S. X.; He, J.; Liu, Y.; Zhang, X. Synthesis and antifungal activities of
600 carabrol ester derivatives. *J. Agric. Food Chem.* **2012**, *60*, 3817-3823.

601 (50) Wang, H.; Ren, S. X.; He, Z. Y.; Wang, D. L.; Yan, X. N.; Feng, J. T.; Zhang, X. Synthesis,
602 antifungal activities and qualitative structure activity relationship of carabrone hydrazone derivatives as
603 potential antifungal agents. *Int. J. Mol. Sci.* **2014**, *15*, 4257-4272.

604 (51) Yu, T. T.; Tian, X. H.; Li, H.; Li, W.; Zhu, W. J.; Zhou, H. P.; Tian, Y. P.; Wu, J. A reversible and

605 highly selective fluorescence "on-off-on" probe for detecting nickel ion in the mitochondria of living
606 cells. *Biosens. Bioelectron.* **2016**, *82*, 93-98.
607 (52) Manders, E. M.; Stap, J.; Brakenhoff, G. J.; van Driel, R.; Aten, J. A. Dynamics of
608 three-dimensional replication patterns during the S-phase, analysed by double labelling of DNA and
609 confocal microscopy. *J. Cell Sci.* **1992**, *103*, 857.

610 **Figure Captions**

611 **Figure 1.** Hypothesis and research techniques used in this study for mitochondrial
612 localization of carabrone in Ggt.

613 **Figure 2.** Fluorescence changes of mycelial cells stained with different concentrations of
614 TTY (0.3, 0.35, 0.4, and 0.8 μM) for various time periods.

615 **Figure 3.** Scanning electron microscopic images of hyphal morphology of Ggt. (a) Healthy
616 hyphae in control Petri plates. (b) and (c) hyphae treated with carabrone (28.45 μg/mL) for
617 7 days. Scale bar: 10 μm.

618 **Figure 4.** Transmission electron microscopic images of hyphal ultrastructure of Ggt. (a and
619 b) Healthy hyphae in control Petri plates. (c, d, e and f) Hyphae treated with carabrone
620 (28.45 μg/mL) for 7 days. Mi: mitochondria. Scale bar: 500 nm for (a), (b), (c) and (f); 2
621 μm for (d) and (e).

622 **Figure 5.** Fluorescence images of hyphae co-stained with TTY, MitoTrackerR Green FM
623 and RedDot™. (a) Bright-field image of the mycelial cells in sample; (b) Image of TTY
624 (emission wavelength, 445 nm); (c) Image of MitoTrackerR Green FM (emission
625 wavelength, 525 nm); (d) Image of RedDot™ (emission wavelength, 690 nm); (e) overlay
626 image of (b and c); (f) overlay image of (b and d); (g) overlay image of (b, c and d); (h)
627 Colocalization profile between TTY and MitoTrackerR Green FM. Scale bar: 2 μm; ×100.

628 **Figure 6.** Confocal immunofluorescence images of hyphae treated with carabrone and
629 co-stained with Anti-Mouse IgG (whole molecule)-FITC, and MitoTrackerR Red CMXRos.
630 (a) Bright-field image of the hyphae; (b) Green emission (520 - 550 nm); (c) Red emission
631 (630 - 660 nm); (d) Overlay image of Anti-Mouse IgG (whole molecule)-FITC and

632 MitoTrackerR Red CMXRos; (e) Overlay image of (a, b and c); (f) Colocalization profile
633 between Anti-Mouse IgG (whole molecule)-FITC and MitoTrackerR Green FM. Scale bar:
634 5 μm; × 60.

635 **Table 1. Antifungal activity of carabrone and TTY against Ggt**

Compounds	EC_{50}[a] (μg/mL)	Slop ± SE	CI_{95}[b]	Chi[c]
Carabrone	28.45	2.15 ± 0.24	25.07-29.01	0.23
TTY	33.68	3.35 ± 0.12	29.14-35.45	0.16

636 [a]effective dose for 50% inhibition compared with the control. [b]95% confidence intervals.

637 [c]Chi-square value, significant at $P < 0.05$ level.

638

639

640 **Table 2. Mitochondrial concentration of Ggt treated with carabrone for 7 days**

Carabrone (μg/mL)	Mitochondrial concentration[a] (mg/mL)
0	1.61 ± 0.024 a
28.45	1.15 ± 0.047 b
49.97	0.97 ± 0.072 c

641 [a]The data of was the average of 3 repetitions; Significant difference at $P < 0.01$ by

642 Duncan's multiple range test.

643

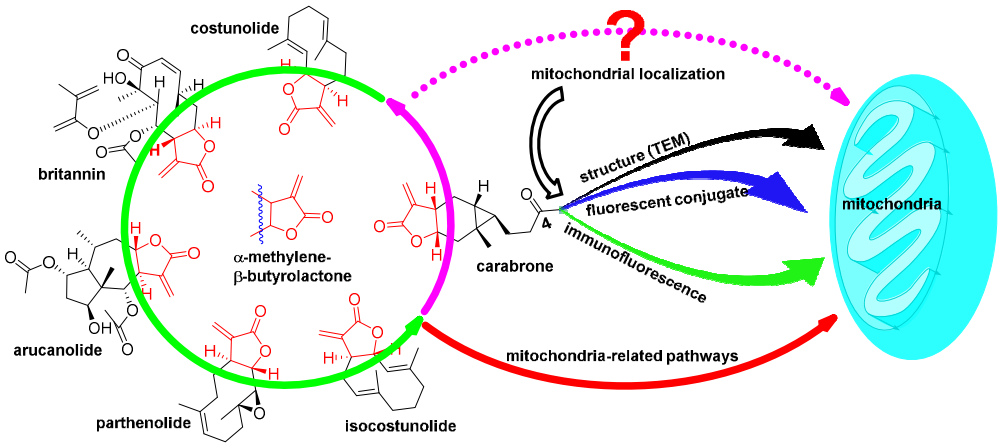

Figure 1. Hypothesis and research techniques used in this study for mitochondrial localization of carabrone in Ggt.

Scheme 1. Synthesis of TTY, T-BSA, and T-OVA

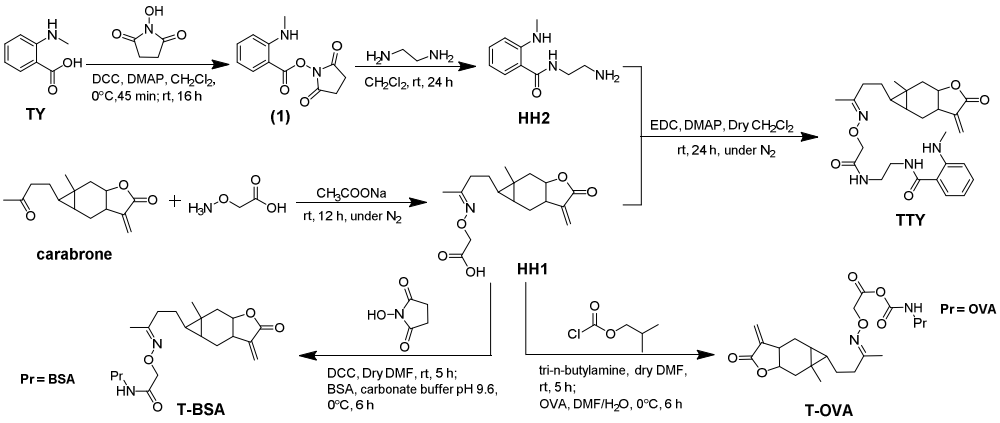

656

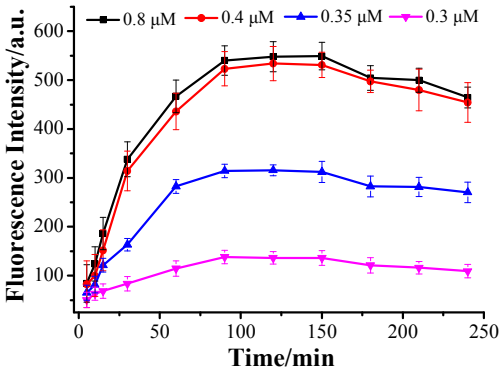

657

658 **Figure 2.** Fluorescence changes of mycelial cells stained with different concentrations of

659 TTY (0.3, 0.35, 0.4, and 0.8 μM) for various time periods.

660

661

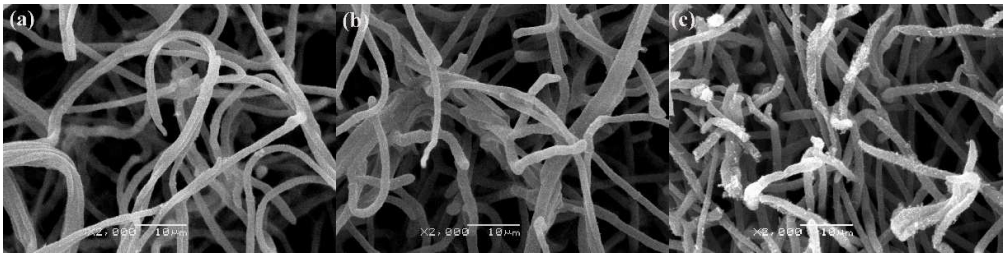

662

663 **Figure 3.** Scanning electron microscopic images of hyphal morphology of Ggt. (a) Healthy

664 hyphae in control Petri plates. (b) and (c) hyphae treated with carabrone (28.45 μg/mL) for

665 7 days. Scale bar: 10 μm.

666

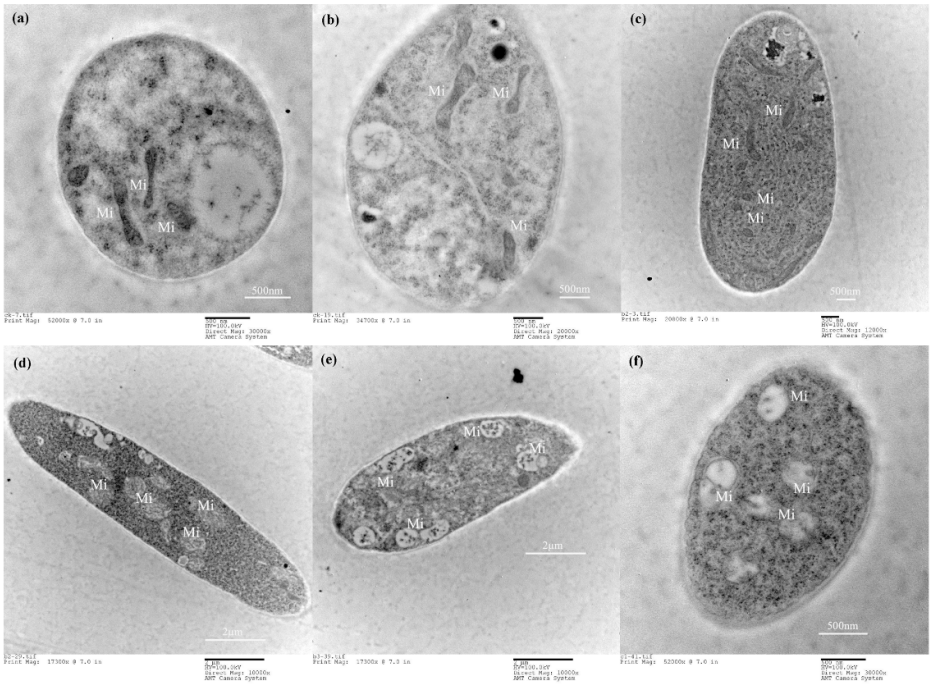

Figure 4. Transmission electron microscopic images of hyphal ultrastructure of Ggt. (a and b) Healthy hyphae in control Petri plates. (c, d, e and f) Hyphae treated with carabrone (28.45 μg/mL) for 7 days. Mi: mitochondria. Scale bar: 500 nm for (a), (b), (c) and (f); 2 μm for (d) and (e).

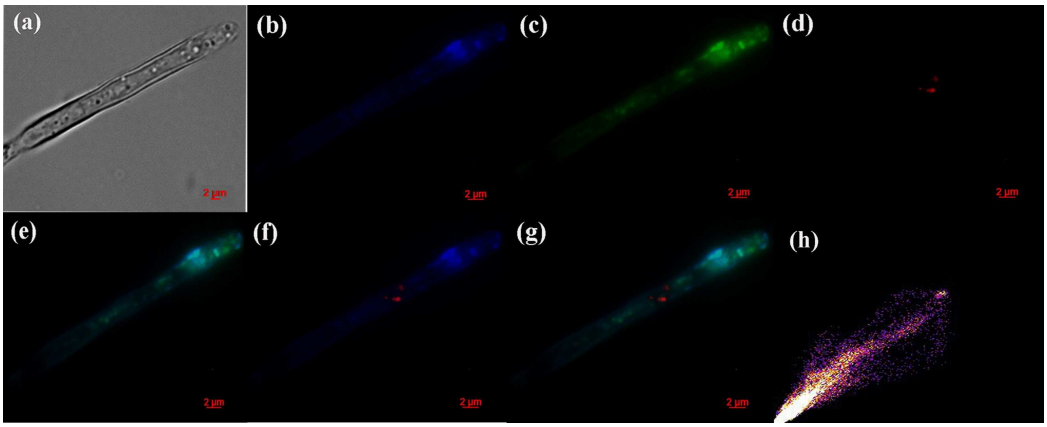

Figure 5. Fluorescence images of hyphae co-stained with TTY, MitoTrackerR Green FM and RedDot™. (a) Bright-field image of the mycelial cells in sample; (b) Image of TTY (emission wavelength, 445 nm); (c) Image of MitoTrackerR Green FM (emission wavelength, 525 nm); (d) Image of RedDot™ (emission wavelength, 690 nm); (e) overlay image of (b and c); (f) overlay image of (b and d); (g) overlay image of (b, c and d); (h) Co-localization profile between TTY and MitoTrackerR Green FM. Scale bar: 2 μm; ×100.

698

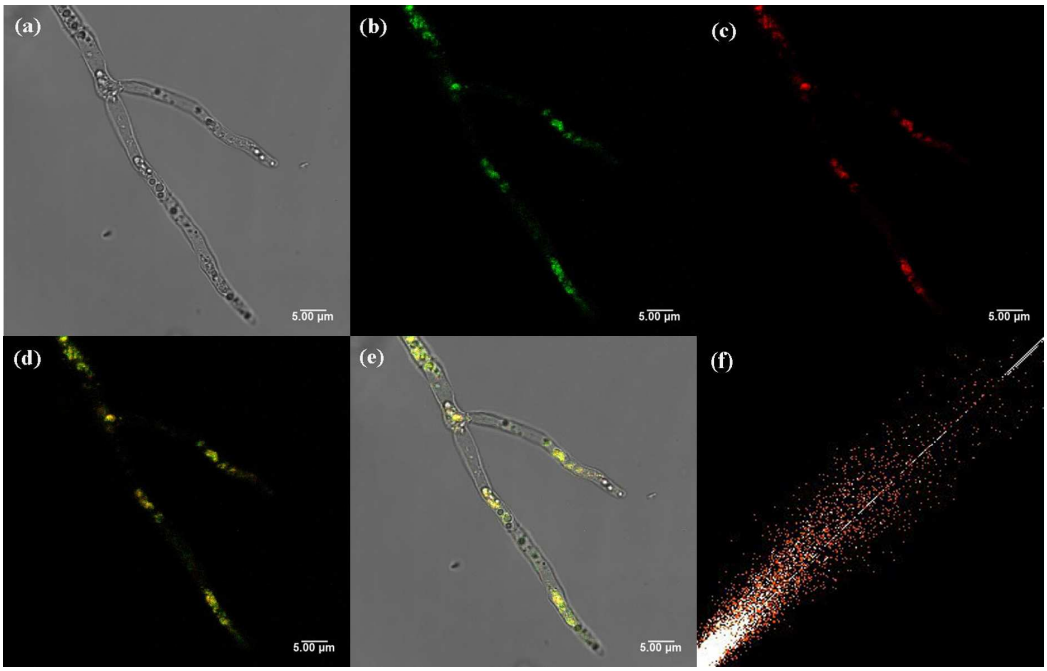

699

700 **Figure 6.** Confocal immunofluorescence images of hyphae treated with carabrone and
701 co-stained with Anti-Mouse IgG (whole molecule)-FITC, and MitoTrackerR Red CMXRos.
702 (a) Bright-field image of the hyphae; (b) Green emission (520 - 550 nm); (c) Red emission
703 (630 - 660 nm); (d) Overlay image of Anti-Mouse IgG (whole molecule)-FITC and
704 MitoTrackerR Red CMXRos; (e) Overlay image of (a, b and c); (f) Co-localization profile
705 between Anti-Mouse IgG (whole molecule)-FITC and MitoTrackerR Green FM. Scale bar:
706 5 µm; × 60.

TOC

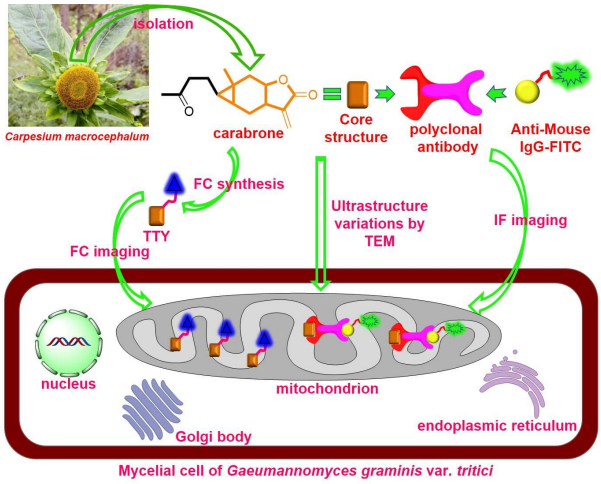
isolation
Carpesium macrocephalum
carabrone
Core structure
polyclonal antibody
Anti-Mouse IgG-FITC
FC synthesis
TTY
FC imaging
Ultrastructure variations by TEM
IF imaging
nucleus
mitochondrion
Golgi body
endoplasmic reticulum
Mycelial cell of Gaeumannomyces graminis var. tritici